Superhydrophobic Hexadecyltrimethoxysilane Modified Fumed Silica Nanostructure / Poly(butyl methacrylate) Composite Thin Films via Aerosol Assisted Deposition: Implications for Self-Cleaning Surfaces

Jiatong Huo[a], Cesar III De Leon Reyes[a], Julie Jalila Kalmoni[a], Seonghyeok Park[b], Gi Byoung Hwang[a], Sanjayan Sathasivam[a,b]* and Claire J. Carmalt[a]*

*Corresponding authors

[a]Materials Chemistry Centre, Department of Chemistry, University College London, 20 Gordon Street, London WC1H 0AJ, UK

[b]School of Engineering, London South Bank University, London SE1 0AA, UK

E-mail: s.sathasivam@lsbu.ac.uk & c.j.carmalt@ucl.ac.uk

Abstract

Superhydrophobic coatings, with their unique nanostructured surface properties, have application in many industrially important technologies but are currently dominated by environmentally problematic fluorinated compounds. Here, we demonstrate the fabrication of fluorocarbon free superhydrophobic coatings consisting of poly(butyl methacrylate) (PBMA) and nanostructured hexadecyltrimethoxysilane (HDTMS) functionalised fumed SiO_2/PBMA as self-cleaning surfaces via a facile ambient pressure aerosol deposition route. X-ray photoelectron and infrared spectroscopy measurements showed successful composite formation. The deposition temperature and HDTMS-SiO_2:PBMA ratio was optimized to give films that had a water contact angle as high as 161±1° and a sliding angle of 1° owing to a hierarchical surface nano- and microstructure and a root mean square surface roughness of 592 nm. This work shows a high through put, single step route to environmentally friendly PBMA based superhydrophobic coatings.

Keywords

Superhydrophobic coatings, Self-cleaning, Nanoparticles, Polymers, Composites, Aerosol assisted deposition

Introduction

A superhydrophobic (SH) surface is one that repels water, more specifically, to a water contact angle (WCA) greater than 150°.[1–3] This phenomenon is widely seen in nature, for example in the leaves of the lotus plant, the wings of the butterfly and the feet of geckos and results in useful self-cleaning and/or water-repellent properties.[4] Superhydrophobicity arises due to two important factors – 1) surface chemistry and 2) surface nano- and micro- roughness. The careful control of these two parameters has enabled the development of artificial SH materials that have applications in, for example, self-cleaning surfaces, oil-water separation, and anti-fogging materials.[5–8]

To achieve the low surface energy necessary for superhydrophobicity in artificial SH surfaces, fluorinated substrates such as polytetrafluoroethylene (PTFE) or fluorinating agents like fluoroalkylsilanes (FAS) are typically used.[9] However, fluorine containing compounds such as these, have sever environmental and economic downsides. Due to the strength of carbon-fluorine bonds, fluorinated polymers are highly stable and resistant to degradation therefore they are known to be persistent and bio-accumulative in the environment.[10] Furthermore, fluorinated polymer-based SH materials tend to be expensive and can be challenging to apply or integrate into existing systems thus limiting the widescale practical application of SH materials.

Recently, there has been a push to develop SH surfaces with more environmentally benign polymers such as polydimethylsiloxane (PDMS) and epoxy resin. [11–13] A common strategy to obtain high WCAs with polymer-based materials is through the use of oxide nanoparticles to increase roughness.[2,12,14] Previously, raw nanoparticles such as ZnO or TiO_2 as well as those functionalised with long chain alkanes, for example, oleic or steric acid have been used with polymers.[12,14–16] SiO_2 is particularly advantageous as it is abundant, inexpensive and, owing to an ultra-wide band gap, photo inactive, therefore causes no polymer degradation issues.[16,17] Furthermore, when SiO_2 particles are functionalised with large organic groups, their dispersion or solubility in solvents increases thus improving their processibility in fabrications techniques such as spin or spray coating. As such, hexadecyltrimethoxysilane (HDTMS) functionalized SiO_2 NPs are highly applicable for the synthesis coatings as they can provide nanoscale roughness and when clustered together can give microscale features – both highly important to achieve superhydrophobicity.

Furthermore, the HDTMS component is hydrophobic and thus helps to maintain the necessary low surface energy of the particle/polymer composite systems.

The fabrication of SH surfaces can take a top-down approach whereby a bulk material is made rough through moulding, machining, and photolithography.[4] The disadvantage to this route is that it is often a multi-step process needing sophisticated tools to carefully produce the necessary morphology.

An alternative approach is the bottom-up method whereby a relatively complex surface with a nano and micro-structure is fabricated from simpler building blocks. Since this approach usually involves an element of self-assembly (i.e., components spontaneously assemble driven by their need to form an energetically stable structure) it is relatively easier, quicker, and cheaper to fabricate.[4] Techniques to achieve this include chemical bath deposition, spin coating and chemical vapor deposition (CVD).[1,7,18,19]

Aerosol assisted chemical vapour deposition (AACVD), a branch of CVD, is a common deposition technique used to deposit functional thin films (Figure 1a).[20–26] The novelty of AACVD is that precursors are transferred to the deposition chamber in the form of aerosol droplets after being dissolved in a suitable solvent. Whereas in traditional CVD the precursors need to have a significant vapour pressure to enter into the gas phase and transfer to the susbtrate. As such the growth of SH coatings via CVD have typically been limited to volatile silane-based precursors such as trimethylmethoxysilane, PDMS or fluoro compounds like hexafluorobutyl acrylate.[27–29] Pure metal oxide SH coatings such as ZnO are also grown via CVD through the thermal volatilisation of precursors.[30] In AACVD there is no such volatility requirement, therefore allowing a wider range of reagents with potentially reduced handling issues, toxicity and cost to be used for film growth. [31] This aerosol assisted route can also be used to grow films from nano- and microparticles and non-volatile polymers with large molecular weights suspended/dissolved in a solvent.[18]

Poly(butyl methacrylate) (PBMA) is an inexpensive and environmentally friendly polymer with an appropriately low surface energy (28.8 mJ/m^2) and glass transition (T_g=20-25 °C) that make it a highly suitable for superhydrophobic applications. In the smooth form, PBMA is hydrophobic with a WCA of 94±2° (See ESI Figure S1).

Extreme water repellence can be achieved by increasing its surface roughness through the use of, for example nanoparticles. [32,33]

Unlike PDMS, PBMA is not well investigated. For example, SH PBMA coatings by Walter *et al.* have shown spray deposited SH coatings based on PBMA with WCAs of ~150°.[34] Another report involves a multi-step process of spray coating, soaking, washing and drying stainless steel meshes with a hybrid of tetrapodal ZnO with various forms of polymethacrylate, including PBMA, resulting in borderline superhydrophobicity (150±5°).[35] Further research on PBMA based SH surfaces is necessary to push their functionality close to what has been achieved using fluorocarbon based systems.

In this paper, we demonstrate for the first time a route to nanostructured superhydrophobic thin films using non-fluorinated and environmentally benign polymer PBMA via aerosol assisted deposition. Pure PBMA films were hydrophobic with a WCA of 113±1º, a 20º increase compared spin coated flat PBMA, due the inherent roughness imparted by the aerosol growth technique. Superhydrophobicity was successfully achieved when PBMA composited with HDTMS-SiO_2 via a single step deposition, resulting in WCAs as high as 161±1° and sliding angles as low as 1°. The WCA obtained in our study is the highest reported to date for PBMA SH coatings and is comparable with values reported for even fluorinated SH materials. Furthermore, the composite films showed excellent self-cleaning properties when tested at a tilt angle of only 1º. The aerosol assisted deposition method detailed here provide opportunities for the development of PBMA based water repelling materials for various applications including as self-cleaning surfaces.

Experimental

Film synthesis

Poly (butyl methacrylate), and toluene (99%) were purchased from Sigma-Aldrich, U.K and Aerosil R816 hexadecyltrimethoxysilane functionalised fumed SiO_2 (HDTMS-SiO_2) from Lawrence Industries. All reagents were used without further purification steps.

AACVD depositions were carried out on a custom built cold-wall reactor where a barrier coated float glass (from NSG^{TM}) was positioned 8 mm above a graphite block containing a Watlow cartridge heater regulated by a Cr-Ni-Al (Type-K) thermocouple (Figure 1a). The reactor was maintained at 200, 250, 350 or 400 ^oC. The precursor solutions were contained in glass bubblers and atomized using a Johnson Matthey Liquifog® piezoelectric ultrasonic humidifier. The aerosol mist was carried into the reactor using a N_2 flow rate of 0.5 L min^{-1}. At the end of the depositions for both systems, the reactor was turned off and cooled under a flow of nitrogen until 100 ^oC after which point the samples were removed. The coated substrates were handled and stored in air.

PBMA coating: PBMA (0.25 g, 0.74 mmol) was dissolved in toluene (30 mL) with the aid of ultrasonic sonication for 10 minutes in glass bubbler. An aerosol mist was generated from this solution and carried over into the reactor using N_2 gas at a flow rate of 0.5 L min^{-1}. Once the solution had been depleted, additional toluene (30 mL) was added to the flask to dissolve any remaining PBMA powder and generate an aerosol mist. The deposition was stopped once the toluene solution had been depleted. Using this procedure, depositions were carried out at a reactor temperature of 200, 250, 350 or 400 °C.

HDTMS-SiO_2/PBMA coating: PBMA (0.25 g, 0.74 mmol) was dissolved in toluene (30 mL) in a glass bubbler with the aid of ultrasonic sonication for 10 minutes. To this solution 0.5, 0.75, 1 or 1.25 g of HDTMS-SiO_2 was added and the mixture was sonicated for a further 10 minutes. An aerosol mist was generated from this solution and carried over into the reactor (at a temperature of 250 ^oC) using N_2 gas at a flow rate of 0.5 L min^{-1}. Once the solution had been depleted, additional toluene (30 mL) was added to the flask to dissolve any remaining HDTMS-SiO_2 and PBMA and

generate an aerosol mist. The deposition was stopped once the toluene solution had been depleted.

Film characterisation

JEOL JSM-7600 Field Emission SEM at an accelerating voltage of 2 keV was used for scanning electron microscopy (SEM) measurements (samples were coated with gold to avoid charging). Fourier transform infrared spectroscopy (FT-IR) were recorded on a Bruker FT-IR Platinum ATR single refection between 400 to 4000 cm^{-1}. The films were removed from the substrate using a stainless-steel knife prior to measurement. X-ray photoelectron spectroscopy (XPS) was performed using a Thermo Scientific Kα photoelectron spectrometer using monochromatic $Al_{k\alpha}$ radiation. Higher resolution scans were recorded for the principal peaks of C(1s), O(1s), Si(2p) at a pass energy of 50 eV. The peaks were fit using Casa XPS software with binding energies adjusted to adventitious carbon (284.5 eV) for charge correction. The error in the quoted binding energy values can be up to ±0.2 eV.

Atomic force microscopy (AFM) was carried out using a Keysight 5500 scanning probe microscope with images recorded in tapping mode with a Si cantilever (NuNano SCOUT-150) at a resonate frequency of ~150 kHz and spring constant of ~18 Nm^{-1}. The root mean square (RMS) was obtained by dividing the measured surface area over the projected area (10 µm x 10 µm). Water contact angles (CA) were measured with a FTÅ 1000 B Class instrument with a 2, 5 and/or 13 µl water droplet. Contact angle hysteresis (CAH) measurements were obtained using a Krüss DSA25E Droplet Shape Analyser using protocol outlined by Huhtamäki *et al* using 23G needle.[36] In brief, an average advancing contact angle (ACA) and receding contact angle (RCA) was calculated by capturing a series of images obtained as a water droplet was slowly dispensed and aspirated (to reduce dynamic effects). CAH was calculated as the difference between the two averaged angles. Optical measurements were carried out using a Shimadzu 3600i Plus spectrometer over a wavelength range of 200 to 1100 nm. The adherence of the coatings to the glass substrate was tested via the tape peel test whereby a fresh portion of sticky tape (Sellotape) was applied to the coating, pressed down and then removed. The WCA was measured after each peal with a total of 10 peels carried out. The self-cleaning test was carried out by tilting the sample to

an angle of 1^{o}, applying glitter on top of the coating to simulate dirt particles and then gently releasing water droplets from a 21G needle at a height of 1 cm.

Results and Discussion

Poly(butyl methacrylate) (PBMA) and hexadecyltrimethoxysilane modified fumed silica nanoparticles (HDTMS-SiO_2) composite superhydrophobic thin films (HDTMS-SiO_2/PBMA) were fabricated using an aerosol assisted chemical vapour deposition (AACVD) reactor which consisted of a glass substrate suspended above a heated carbon block (Figure 1a). Due to nucleation and relatively large PBMA or HDTMS-SiO_2/PBMA particle formation in the gas phase, thermophoretic forces drive the deposition to take place on the suspended glass substrate which is cooler than the carbon block.[37,38] This thermophoresis driven film growth allows for the PBMA based films to have hierarchical structure that is advantageous for hydrophobicity (Figure 1b).

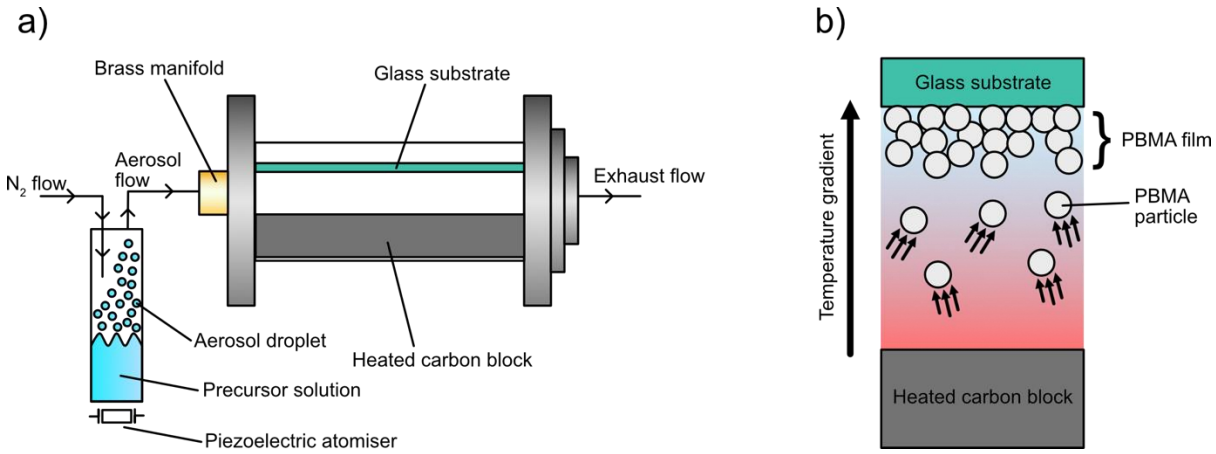

Figure 1: a) A schematic of the AACVD set up used to grow the PBMA based films and b) diagram showing the thermophoretic effect driven PBMA based film formation.

In these films, the PBMA polymer serves as a dual purpose 1) by providing a chemically stable, relatively low surface free energy (28.8 mJ/m^2) substrate and 2) acts as an adhesive for additives such as hydrophobic HDTMS-SiO_2 nanoparticles that help to increase the surface roughness and therefore superhydrophobicity.[33] The films were produced from a toluene solution of PBMA or HDTMS-SiO_2 and PBMA with an N_2 carrier gas with a flow rate of 0.5 L min^{-1}. Toluene was selected as the solvent in this study due to its ability to fully dissolve PBMA across a wide temperature range (0 – 110.6 ^oC) and therefore minimise any blockages in the reactor during film growth.[39] Other solvents that are more environmentally and industrially friendly include isopropanol and ethanol although the solubility of PBMA has a narrower temperature range of 22-110.6 ^oC and 42-110.6 ^oC, respectively. [39]

The optimal reactor temperature to achieve maximum water contact angles (WCA) was determined to be 250 °C (Figure 2a). At 200 °C, little and discontinuous PBMA film growth took place evidenced by the lack of material morphology seen via SEM (see ESI Figure S2) and a WCA of 82±9° which is below that of flat PBMA via spin coating at 94±2° (see ESI Figure S1). Above 250 °C, there was no significant increase in the water repulsion ability, presumably due to the observed no meaningful change in surface morphology (see ESI Figure S2). Therefore, all proceeding depositions were carried out at 250 °C in an effort to be minimize energy expenditure. For the HDTMS-SiO_2/PBMA composite films, the concentration of HDTMS-SiO_2 in the precursor solution was varied to determine its influence on the WCA (see ESI Figure S3). A 3:1 ratio (HDTMS-SiO_2:PBMA) was found to yield the highest WCA. Any further increase in HDTMS-SiO_2 caused no significant change (Figure 2b), therefore only the 3:1 HDTMS-SiO_2:PBMA films were studied further, herein referred to as HDTMS-SiO_2/PBMA.

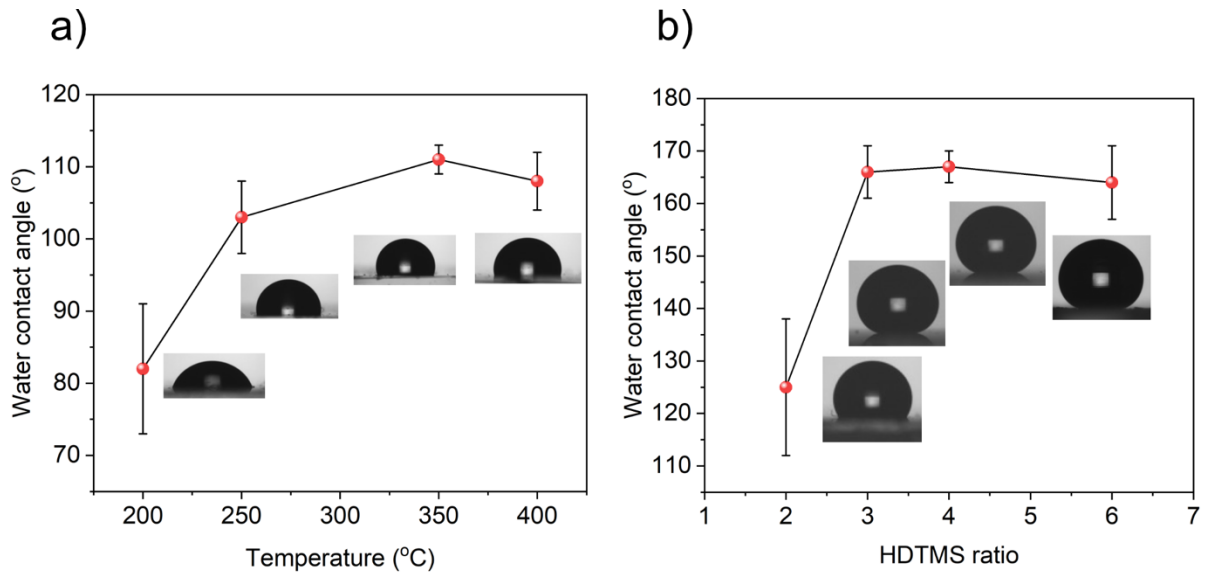

Figure 2: a) change in WCA with increasing reactor temperature for the pure PBMA film and b) change in WCA with increasing HDTMS-SiO_2:PBMA ratio. All measurements taken using a 13 µL water droplet.

FTIR and X-ray photoelectron spectroscopy (XPS) analysis was carried out to confirm successful incorporation of HDTMS-SiO_2 and to monitor decomposition to PBMA during the AACVD process (Figure 3a). The FTIR spectrum for the pure PBMA film showed signature peaks at 2957.5 cm^{-1} and 1721.4 cm^{-1} corresponding to stretching vibrations of the alkane C-H and C=O present in the ester components as also observed in the PBMA powder precursor.[40] For the HDTMS-SiO_2/PBMA films,

additional peaks at 1082.2 cm^{-1} and 805.2 cm^{-1} were observed corresponding to the asymmetric stretching Si-O-Si and the Si-O bending vibrations (respectively) of the of the HDTMS-SiO_2 particles. [41–44] A peak associated to the bending vibration of O-Si-O at 467.0 cm^{-1} in the particles was also observed. These peaks were also observed in the starting material spectrum of the HDTMS-SiO_2 powder. The presence of peaks matching those found in the starting material and the lack of additional new peaks suggests the formation of HDTMS-SiO_2/PBMA films without decomposition. This was further confirmed by XPS analysis (Figure 3b-3f). For the PBMA film, the C 1s signal was best fit with three peaks corresponding to aliphatic C-C/C-H (284.5±0.2 eV), C-O (288.5±0.2 eV) and C=O (286.2±0.2 eV) likely from the ester component of PBMA.[45–47] These three peaks were also observed for the HDTMS-SiO_2/PBMA films at binding energies of 284.5±0.2 eV, 288.3±0.2 eV and 286.0±0.2 eV. The O 1s experimental data for both sets of films showed an asymmetric line shape. The O 1s spectrum from the PBMA film was fit with only two environments C=O and C-O at 530.8±0.2 eV and 533.0±0.2 eV, respectively.[47,48] For the HDTMS-SiO_2/PBMA film, along with these ester oxygen environments, an additional peak at 532.5±0.2 eV belonging to the Si-O bonds of the fumed silica particles was observed, confirming successful composite formation. The asymmetric Si 2p signal for the composite film was fit with a pair of doublets. The Si $2p_{3/2}$ peak centred at 103.0±0.2 eV was assigned to Si-O with a composition of 83.4% whereas the significantly smaller (16.6%) secondary Si $2p_{3/2}$ peak at 101.4±0.2 eV matched to Si-C bonds present in HDTMS.[14]

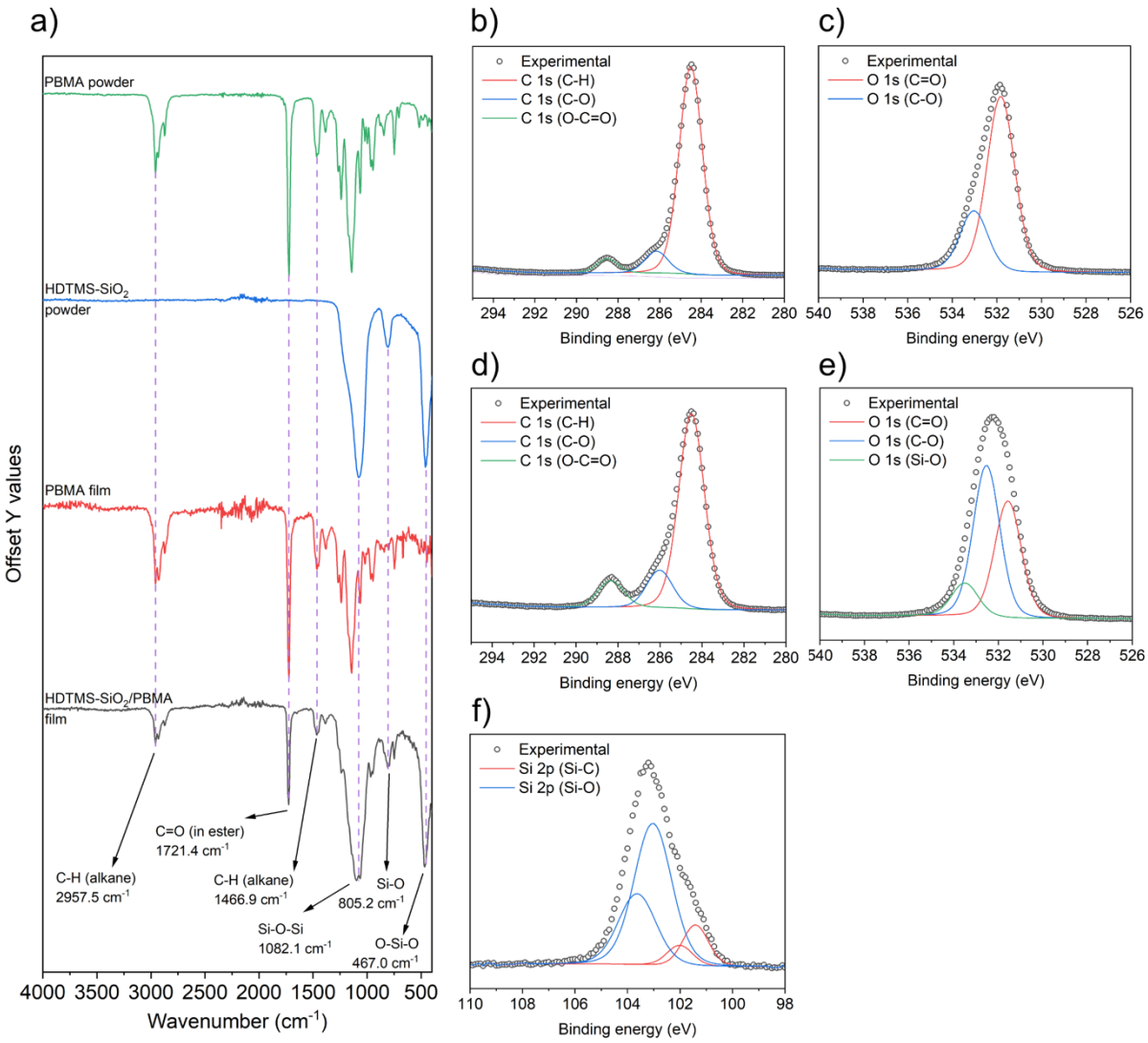

Figure 3: a) FTIR spectra showing the signature vibrations in the PBMA and HDTMS-SiO_2 starting material powders and films. XPS data showing the fittings for b) C 1s c) O 1s spectra for the PBMA film and d) C 1s, e) O 1s and f) Si 2p spectra for the HDTMS-SiO_2/PBMA film.

Scanning electron microscopy (SEM) and atomic force microscopy (AFM) were carried out on the PBMA and HDTMS-SiO_2/PBMA films to see the surface morphology and determine the surface roughness (Figure 4). The pure PBMA surface consisted of irregular domes, one to 10 microns in diameter (Figure 4a, b & c) as well some smaller protrusions in the nanometre scale. The PBMA film thickness, as determined by side on SEM was 1 μm across the measured area. The root mean square (RMS), often determined by atomic force microscopy (AFM) or surface profilometry, provides a quantitative measure of a surface by quantifying the variation in height of the surface.[49] The AFM determined RMS for the PBMA film was 207 nm (Figure 4d & e). However, for the HDTMS-SiO_2/PBMA film, it was almost three times as high at 592 nm (Figure 4i & j). This is also evident from the hierarchical structure observed in the SEM images

of the composite film (Figure 4f, g & h) compared to the pure PBMA sample. Side on SEM revealed the composite film to be up to 3 μm in thickness.

The protrusions densely cover the surface of the substrate and vary in size from hundreds of nanometres to several micrometres. A closer look at these structures in the HDTMS-SiO_2/PBMA film also reveals the nanoscale roughness induced by the silica particles (Figure 4g and h). The hierarchical morphology and surface roughness of the HDTMS-SiO_2/PBMA film observed in this study is comparable to literature findings for composite films of metal oxide NPs/PDMS/ and metal oxide NPs/PDMS/epoxy resin.[12,14,50–52]

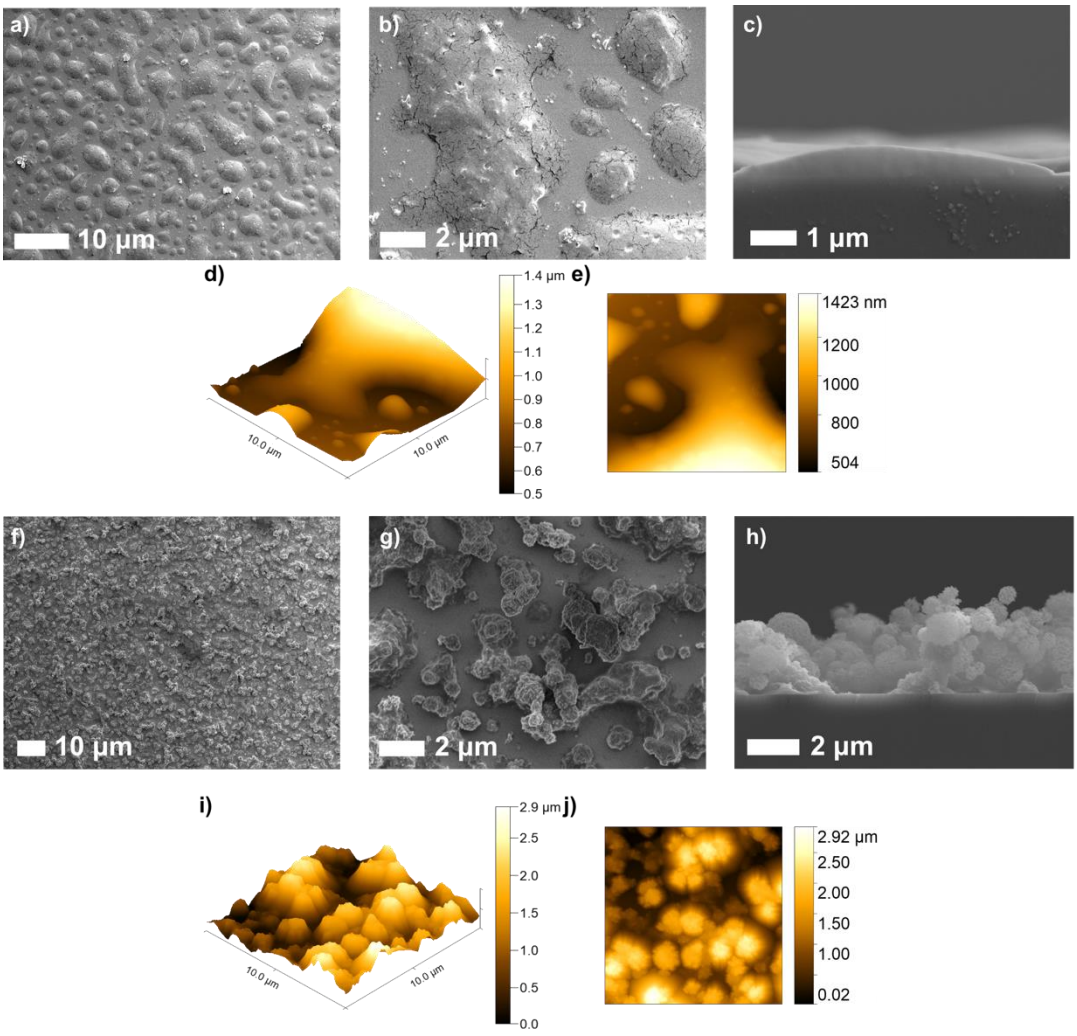

Figure 4: Top down and side on SEM images of the PBMA (a, b and c) and HDTMS-SiO_2/PBMA (f, g and h) showing the change in morphology upon the introduction of HDTMS-SiO_2 particles as well as the film thickness. AFM data used to determine the surface roughness is also shown for d and e) the pure and I and j) composite film.

UV-visible-near infrared (UV-Vis-NIR) spectroscopy was carried out on the films in transmittance mode (Figure 5). The PBMA film had an average transmittance in the

visible wavelengths (400-700 nm) at 20.5% whereas as the HDTMS-SiO_2/PBMA sample was at 8.6%. The poor optical transmittance of the films is associated to their high surface roughness and feature sizes being similar to or greater than the wavelength of incident light. At this scale, Mie scattering takes place and increases exponentially with increasing particle size.[53] This is in line with a previous theoretical modelling study by Cho *et al.* where they have shown how a RMS roughness >200 nm can significantly reduce the optical transparency of SH coatings based on SiO_2 nanoparticle.[49]

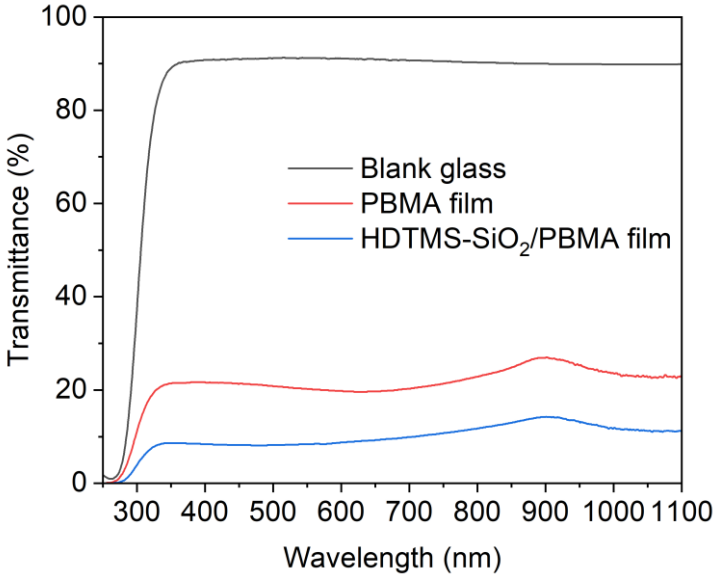

Figure 5: UV-vis spectra showing transmittance for the blank glass substrate, PBMA and HDTMS-SiO_2/PBMA films.

Water contact angle (WCA) measurements were carried out on both films to determine their water repellence properties. The pure PBMA film was hydrophobic with a WCA of 113±1° (Figure 6a and Table 1), this is higher than that of flat pure PBMA grown via spin coating (94±2°) due to the inherent roughness imparted onto polymer films via the aerosol deposition process.[15,54] The incorporation of HDTMS functionalised silica nanoparticles was able to further increase the surface roughness, resulting in WCAs for the HDTMS-SiO_2/PBMA composite film of 161±1° (Figure 6b and Table 1). The WCA for the aerosol deposited HDTMS-SiO_2/PBMA film is significantly higher than previous reports of PBMA/silica films with hierarchical topographies produced by spray coating which gave WCAs of ~150°.[34] This could be due to the difference in the of micro to nano scale roughness ratios that seems to be evident when the SEM images are compared. The spray deposited films appear to have a lower micro to nano

roughness ratio relative to our aerosol deposited HDTMS-SiO_2/PBMA films possibly due to the differences in growth temperature.

The HDTMS-SiO_2/PBMA grown in our study also show comparable WCAs to PDMS and metal oxide NP composites. For example, a WCA of 162° was seen by Crick *et al*. for SH TiO_2/PDMS films grown via AACVD with a surface morphology consisting of 3-5 µm protrusions.[12] SiO_2/PDMS films grown on magnesium alloy substrates by Xie *et al*. with RMS values of ~150-190 nm were reported to give WCAs of 153.6°.[55]

Contact angle hysteresis (CAH), a measure of the difference between the advancing and receding angles of a water droplet, of the PBMA and composite films were 26±8° and 14±7°, respectively (Table 1).

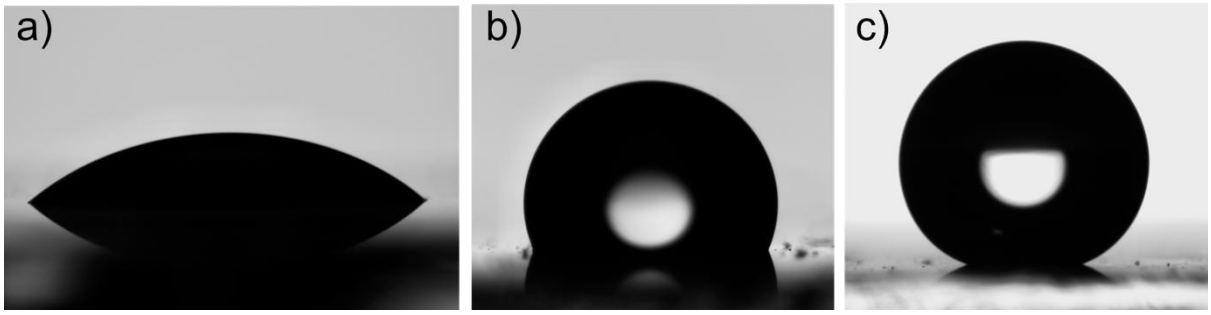

Figure 6: 5 µL water droplets sitting on the surface of a) glass substrate, b) PBMA and c) HDTMS-SiO_2/PBMA films giving WCAs of 41±3°, 113±1° and 161±1°.

Table 1: Table of water contact, advancing contact angle, receding contact angle, contact angle hysteresis and sliding angle results for the PBMA and HDTMS-SiO_2/PBMA films using a 5 µL droplet volume.

Film	Water contact angle (°)	Advancing contact angle (º)	Receding contact angle (º)	Contact angle hysteresis (°)	Sliding angle (°)
Glass	41± 3	N/A	N/A	N/A	N/A
PBMA	113±1	114±1	88±8	26±8	N/A
HDTMS-SiO_2/PBMA	161±1	161±1	147±7	14±7	1

Due the water droplet stubbornly sticking to the PBMA even when upside down, no sliding angle measurements were possible. The sliding angle for the HDTMS-SiO_2/PBMA film was measured to be 1° (Figure 7a). The combination of high-water

contact angle and a low sliding angle allows the HDTMS-SiO_2/PBMA films to have application as self-cleaning coatings. The self-cleaning properties of the composite film were tested at a tilt angle of 1°, with glitter to simulate dirt particles and water droplets being released via a needle from a height of 1 cm (Figure 7b). The self-cleaning ability of the composite film is attributed to the higher adhesion force between the water and the dirt (glitter) than water and the composite film, thus water would much rather stick to the dirt and pull it away from the coating during the rolling motion.[14,56–58]

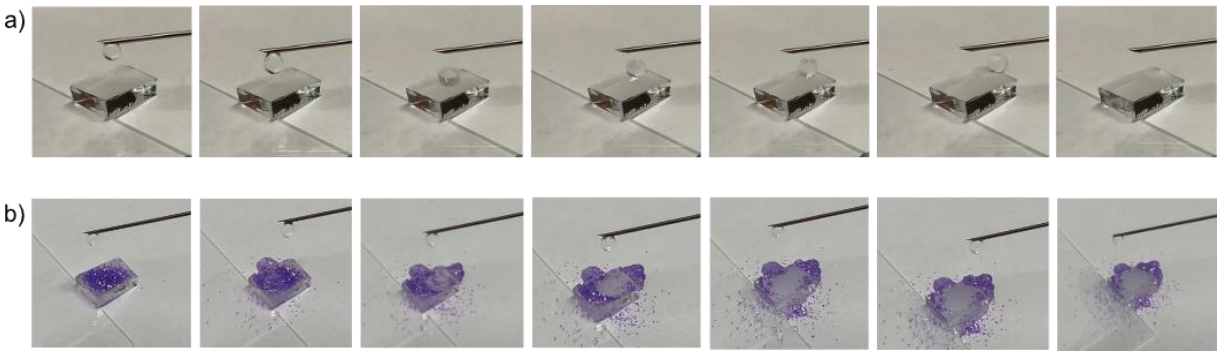

Figure 7: a) Showing a water droplet rolling off on the HDTMS-SiO_2/PBMA film at a tilt angle of 1°. b) the self-cleaning properties of the composite film where the rolling action of water droplets are able to remove glitter from the surface of the film at a tilt angle of 1°.

The adhesion strength of the HDTMS-SiO_2/PBMA films were measured via the peel-tape test.[59] After 10 cycles of the peel test, the WCA was reduced to 107±1° (SEE ESI Figure S4) suggesting the water repellence property of the films was reduced to that of the pure PBMA polymer (113±1°). This suggest the PBMA component of the composite films are well adhered to the substrate, the observed reduction in WCA is most likely due to the removal of the surface HDTMS-SiO_2 NPs.

Conclusion

We report the growth of non-fluorocarbon based superhydrophobic coatings with a water contact angle of 161±1° and a sliding angle of 1° based on a nanostructured composite of HDTMS-SiO_2/PBMA. The WCA reported here is the highest WCA to date for a PBMA based SH surface. The films were grown using an aerosol assited deposition route from a precursor solution consisting of commercially available reagents – PBMA and HDTMS functionalised SiO_2 nanoparticles. Here, the highly flexible PBMA behaved as a low surface energy adhesive for the hydrophobic HDTMS-SiO_2 nanoparticles that were used primarily to increase the surface roughness. FTIR showed that with a relatively low growth temperature of 250 °C, no decomposition of the PBMA nor HDTMS-SiO_2 was observed. SEM highlighted the dense hierarchical nanostructure whilst AFM measurements showed the HDTMS-SiO_2/PBMA films had a RMS roughness of 592 nm. The low sliding angles allow the films to have self-application as self-cleaning surfaces, evidenced by effective cleaning off glitter at a tilt angle of just 1^o.

Acknowledgments

S.S wishes to thank The School of Engineering, London South Bank University for S.P's PhD studentship.

Supporting Information

Flat PBMA film methodology, SEM images, water contact angles, tape peel test results

Author Information

Corresponding authors

Sanjayan Sathasivam - School of Engineering, London South Bank University, London SE1 0AA, UK & Materials Chemistry Centre, Department of Chemistry, University College London, 20 Gordon Street, London WC1H 0AJ, UK; https://orcid.org/0000-0002-5206-9558

Claire J Carmalt – Materials Chemistry Centre, Department of Chemistry, University College London, 20 Gordon Street, London WC1H 0AJ, UK; https://orcid.org/0000-0003-1788-6971;

Jiatong Huo - Materials Chemistry Centre, Department of Chemistry, University College London, 20 Gordon Street, London WC1H 0AJ, UK; https://orcid.org/0009-0000-6446-1728

Cesar III De Leon Reyes - Materials Chemistry Centre, Department of Chemistry, University College London, 20 Gordon Street, London WC1H 0AJ, UK; https://orcid.org/0009-0008-9859-9213

Julie Jalila Kalmoni - Materials Chemistry Centre, Department of Chemistry, University College London, 20 Gordon Street, London WC1H 0AJ, UK; https://orcid.org/0009-0000-0245-5023

Seonghyeok Park - School of Engineering, London South Bank University, London SE1 0AA, UK;

Gi Byoung Hwang - Materials Chemistry Centre, Department of Chemistry, University College London, 20 Gordon Street, London WC1H 0AJ, UK; https://orcid.org/0000-0003-0874-8390

References

(1) Ma, M.; Hill, R. M. Superhydrophobic Surfaces. *Curr Opin Colloid Interface Sci* **2006**, *11* (4), 193–202.

(2) Lu, Y.; Sathasivam, S.; Song, J.; Crick, C. R.; Carmalt, C. J.; Parkin, I. P. Robust Self-Cleaning Surfaces That Function When Exposed to Either Air or Oil. *Science (1979)* **2015**, *347* (6226). https://doi.org/10.1126/science.aaa0946.

(3) Butt, H.-J.; Roisman, I. V; Brinkmann, M.; Papadopoulos, P.; Vollmer, D.; Semprebon, C. Characterization of Super Liquid-Repellent Surfaces. *Curr Opin Colloid Interface Sci* **2014**, *19* (4), 343–354.

(4) Li, X.-M.; Reinhoudt, D.; Crego-Calama, M. What Do We Need for a Superhydrophobic Surface? A Review on the Recent Progress in the Preparation of Superhydrophobic Surfaces. *Chem Soc Rev* **2007**, *36* (8), 1350–1368.

(5) Li, Y.; Shi, B.; Luan, X.; Hao, Z.; Wang, Y. Robust Superhydrophobic/Superoleophilic Filter Paper with TiO2 Nanoparticles for Separating Oil–Water Mixtures and Surfactant-Stabilized Water–Oil Emulsions. *ACS Appl Nano Mater* **2022**, *5* (11), 16687–16693.

(6) Shang, M.; Samuel, M. S.; Biswas, S.; Niu, J. Dual-Layered SiO2 Nanoparticles and Epoxy Polymers for Self-Cleaning Coatings on Ceramic Glaze. *ACS Appl Nano Mater* **2022**, *5* (10), 15934–15941.

(7) Farhadi, S.; Farzaneh, M.; Kulinich, S. A. Anti-Icing Performance of Superhydrophobic Surfaces. *Appl Surf Sci* **2011**, *257* (14), 6264–6269.

(8) Nguyen, N. N.; Davani, S.; Asmatulu, R.; Kappl, M.; Berger, R.; Butt, H.-J. Nano-Capillary Bridges Control the Adhesion of Ice: Implications for Anti-Icing via Superhydrophobic Coatings. *ACS Appl Nano Mater* **2022**, *5* (12), 19017–19024.

(9) Bayer, I. S. Superhydrophobic Coatings from Ecofriendly Materials and Processes: A Review. *Adv Mater Interfaces* **2020**, *7* (13), 2000095.

(10) Stahl, T.; Mattern, D.; Brunn, H. Toxicology of Perfluorinated Compounds. *Environ Sci Eur* **2011**, *23* (1), 38.

(11) Liu, Y.; Sun, R.; Jin, B.; Li, T.; Yao, L.; Feng, L.; He, J. Superhydrophobic VO2 Nanoparticle/PDMS Composite Films as Thermochromic, Anti-Icing, and Self-Cleaning Coatings. *ACS Appl Nano Mater* **2022**, *5* (4), 5599–5608.

(12) Crick, C. R.; Bear, J. C.; Kafizas, A.; Parkin, I. P. Superhydrophobic Photocatalytic Surfaces through Direct Incorporation of Titania Nanoparticles into a Polymer Matrix by Aerosol Assisted Chemical Vapor Deposition. *Advanced Materials* **2012**, *24* (26), 3505–3508.

(13) Kalmoni, J. J.; Heale, F. L.; Blackman, C. S.; Parkin, I. P.; Carmalt, C. J. A Single-Step Route to Robust and Fluorine-Free Superhydrophobic Coatings via Aerosol-Assisted Chemical Vapor Deposition. *Langmuir* **2023**.

(14) Park, S.; Huo, J.; Shin, J.; Heo, K. J.; Kalmoni, J. J.; Sathasivam, S.; Hwang, G. B.; Carmalt, C. J. Production of an EP/PDMS/SA/AlZnO Coated Superhydrophobic Surface through an Aerosol-Assisted Chemical Vapor Deposition Process. *Langmuir* **2022**, *38* (25), 7825–7832.

(15) Crick, C. R.; Parkin, I. P. A Single Step Route to Superhydrophobic Surfaces through Aerosol Assisted Deposition of Rough Polymer Surfaces: Duplicating the Lotus Effect. *J Mater Chem* **2009**, *19* (8), 1074–1076.

(16) Ebert, D.; Bhushan, B. Transparent, Superhydrophobic, and Wear-Resistant Coatings on Glass and Polymer Substrates Using SiO2, ZnO, and ITO Nanoparticles. *Langmuir* **2012**, *28* (31), 11391–11399.

(17) Nekrashevich, S. S.; Gritsenko, V. A. Electronic Structure of Silicon Dioxide (a Review). *Physics of the Solid State* **2014**, *56*, 207–222.

(18) Pi, P.; Hou, K.; Zhou, C.; Li, G.; Wen, X.; Xu, S.; Cheng, J.; Wang, S. Superhydrophobic Cu2S@ Cu2O Film on Copper Surface Fabricated by a Facile Chemical Bath Deposition Method and Its Application in Oil-Water Separation. *Appl Surf Sci* **2017**, *396*, 566–573.

(19) Xu, L.; Karunakaran, R. G.; Guo, J.; Yang, S. Transparent, Superhydrophobic Surfaces from One-Step Spin Coating of Hydrophobic Nanoparticles. *ACS Appl Mater Interfaces* **2012**, *4* (2), 1118–1125.

(20) Chadwick, N.; Sathasivam, S.; Kafizas, A.; Bawaked, S. M.; Obaid, A. Y.; Al-Thabaiti, S.; Basahel, S. N.; Parkin, I. P.; Carmalt, C. J. Combinatorial Aerosol Assisted Chemical Vapour Deposition of a Photocatalytic Mixed SnO<inf>2</Inf>/TiO<inf>2</Inf> Thin Film. *J Mater Chem A Mater* **2014**, *2* (14). https://doi.org/10.1039/c4ta00545g.

(21) Sathasivam, S.; Arnepalli, R. R.; Kumar, B.; Singh, K. K.; Visser, R. J.; Blackman, C. S.; Carmalt, C. J. Solution Processing of GaAs Thin Films for Photovoltaic Applications. *Chemistry of Materials* **2014**, *26* (15), 4419–4424. https://doi.org/10.1021/cm501280e.

(22) Jiamprasertboon, A.; Powell, M. J.; Dixon, S. C.; Quesada-Cabrera, R.; Alotaibi, A. M.; Lu, Y.; Zhuang, A.; Sathasivam, S.; Siritanon, T.; Parkin, I. P.; Carmalt, C. J. Photocatalytic and Electrically Conductive Transparent Cl-Doped ZnO Thin Films: Via Aerosol-Assisted Chemical Vapour Deposition. *J Mater Chem A Mater* **2018**, *6* (26). https://doi.org/10.1039/c8ta01420e.

(23) Tombesi, A.; Li, S.; Sathasivam, S.; Page, K.; Heale, F. L.; Pettinari, C.; Carmalt, C. J.; Parkin, I. P. Aerosol-Assisted Chemical Vapour Deposition of Transparent Superhydrophobic Film by Using Mixed Functional Alkoxysilanes. *Sci Rep* **2019**, *9* (1). https://doi.org/10.1038/s41598-019-43386-1.

(24) Li, S.; Page, K.; Sathasivam, S.; Heale, F.; He, G.; Lu, Y.; Lai, Y.; Chen, G.; Carmalt, C. J.; Parkin, I. P. Efficiently Texturing Hierarchical Superhydrophobic Fluoride-Free Translucent Films by AACVD with Excellent Durability and Self-Cleaning Ability. *J Mater Chem A Mater* **2018**, *6* (36). https://doi.org/10.1039/c8ta05402a.

(25) Palgrave, R. G.; Parkin, I. P. Aerosol Assisted Chemical Vapor Deposition Using Nanoparticle Precursors: A Route to Nanocomposite Thin Films. *J Am Chem Soc* **2006**, *128* (5), 1587–1597.

(26) Hou, X.; Choy, K. Processing and Applications of Aerosol-assisted Chemical Vapor Deposition. *Chemical vapor deposition* **2006**, *12* (10), 583–596.

(27) Ishizaki, T.; Hieda, J.; Saito, N.; Saito, N.; Takai, O. Corrosion Resistance and Chemical Stability of Super-Hydrophobic Film Deposited on Magnesium Alloy AZ31 by Microwave Plasma-Enhanced Chemical Vapor Deposition. *Electrochim Acta* **2010**, *55* (23), 7094–7101.

(28) Mosayebi, E.; Azizian, S.; Noei, N. Preparation of Robust Superhydrophobic Sand by Chemical Vapor Deposition of Polydimethylsiloxane for Oil/Water Separation. *Macromol Mater Eng* **2020**, *305* (12), 2000425.

(29) Şakalak, H.; Yılmaz, K.; Gürsoy, M.; Karaman, M. Roll-to Roll Initiated Chemical Vapor Deposition of Super Hydrophobic Thin Films on Large-Scale Flexible Substrates. *Chem Eng Sci* **2020**, *215*, 115466.

(30) Liu, H.; Feng, L.; Zhai, J.; Jiang, L.; Zhu, D. Reversible Wettability of a Chemical Vapor Deposition Prepared ZnO Film between Superhydrophobicity and Superhydrophilicity. *Langmuir* **2004**, *20* (14), 5659–5661.

(31) Hou, X.; Choy, K. Processing and Applications of Aerosol-assisted Chemical Vapor Deposition. *Chemical vapor deposition* **2006**, *12* (10), 583–596.

(32) Stetsyshyn, Y.; Raczkowska, J.; Lishchynskyi, O.; Awsiuk, K.; Zemla, J.; Dąbczyński, P.; Kostruba, A.; Harhay, K.; Ohar, H.; Orzechowska, B. Glass Transition in Temperature-Responsive Poly (Butyl Methacrylate) Grafted Polymer Brushes. Impact of Thickness and Temperature on Wetting, Morphology, and Cell Growth. *J Mater Chem B* **2018**, *6* (11), 1613–1621.

(33) Nielsen, B. V; Nevell, T. G.; Barbu, E.; Smith, J. R.; Rees, G. D.; Tsibouklis, J. Multifunctional Poly (Alkyl Methacrylate) Films for Dental Care. *Biomedical Materials* **2011**, *6* (1), 015003.

(34) Walter, T.; Hein, T.; Weichselgartner, M.; Wommer, K.; Aust, M.; Vogel, N. Dispersion-Based, Scalable Fabrication of Repellent Superhydrophobic and Liquid-Infused Coatings under Ambient Conditions. *Green Chemistry* **2022**, *24* (7), 3009–3016.

(35) Li, C.; Lee, B.; Wang, C.; Bajpayee, A.; Douglas, L. D.; Phillips, B. K.; Yu, G.; Rivera-Gonzalez, N.; Peng, B.; Jiang, Z. Photopolymerized Superhydrophobic Hybrid Coating Enabled by Dual-Purpose Tetrapodal ZnO for Liquid/Liquid Separation. *Mater Horiz* **2022**, *9* (1), 452–461.

(36) Huhtamäki, T.; Tian, X.; Korhonen, J. T.; Ras, R. H. A. Surface-Wetting Characterization Using Contact-Angle Measurements. *Nat Protoc* **2018**, *13* (7), 1521–1538.

(37) Ashraf, S.; Blackman, C. S.; Palgrave, R. G.; Parkin, I. P. Aerosol-Assisted Chemical Vapour Deposition of WO3 Thin Films Using Polyoxometallate

Precursors and Their Gas Sensing Properties. *J Mater Chem* **2007**, *17* (11), 1063–1070.

(38) Fotiadis, D. I.; Jensen, K. F. Thermophoresis of Solid Particles in Horizontal Chemical Vapor Deposition Reactors. *J Cryst Growth* **1990**, *102* (4), 743–761. https://doi.org/https://doi.org/10.1016/0022-0248(90)90838-C.

(39) Sander, U.; Wolf, B. A. Solubility of Poly (N-alkylmethacrylate) s in Hydrocarbons and in Alcohols. *Die Angewandte Makromolekulare Chemie: Applied Macromolecular Chemistry and Physics* **1986**, *139* (1), 149–156.

(40) Suhailath, K.; Ramesan, M. T.; Naufal, B.; Periyat, P.; Jasna, V. C.; Jayakrishnan, P. Synthesis, Characterisation and Flame, Thermal and Electrical Properties of Poly (n-Butyl Methacrylate)/Titanium Dioxide Nanocomposites. *Polymer Bulletin* **2017**, *74*, 671–688.

(41) Xu, B.; Zhang, Q. Preparation and Properties of Hydrophobically Modified Nano-SiO2 with Hexadecyltrimethoxysilane. *ACS Omega* **2021**, *6* (14), 9764–9770.

(42) Wu, G.; Liu, D.; Chen, J.; Liu, G.; Kong, Z. Preparation and Properties of Super Hydrophobic Films from Siloxane-Modified Two-Component Waterborne Polyurethane and Hydrophobic Nano SiO2. *Prog Org Coat* **2019**, *127*, 80–87.

(43) Zhang, H.; Li, B.; Sun, D.; Miao, X.; Gu, Y. SiO2-PDMS-PVDF Hollow Fiber Membrane with High Flux for Vacuum Membrane Distillation. *Desalination* **2018**, *429*, 33–43.

(44) Beganskienė, A.; Sirutkaitis, V.; Kurtinaitienė, M.; Juškėnas, R.; Kareiva, A. FTIR, TEM and NMR Investigations of Stöber Silica Nanoparticles. *Mater Sci (Medžiagotyra)* **2004**, *10*, 287–290.

(45) Affrossman, S.; Jérôme, R.; O'neill, S. A.; Schmitt, T.; Stamm, M. Surface Structure of Thin Film Blends of Polystyrene and Poly (n-Butyl Methacrylate). *Colloid Polym Sci* **2000**, *278*, 993–999.

(46) Biesinger, M. C. Accessing the Robustness of Adventitious Carbon for Charge Referencing (Correction) Purposes in XPS Analysis: Insights from a Multi-User Facility Data Review. *Appl Surf Sci* **2022**, *597*, 153681.

(47) Louette, P.; Bodino, F.; Pireaux, J.-J. Poly (Butyl Methacrylate)(PBMA) XPS Reference Core Level and Energy Loss Spectra. *Surface science spectra* **2005**, *12* (1), 139–143.

(48) López, G. P.; Castner, D. G.; Ratner, B. D. XPS O 1s Binding Energies for Polymers Containing Hydroxyl, Ether, Ketone and Ester Groups. *Surface and interface analysis* **1991**, *17* (5), 267–272.

(49) Cho, K. L.; Liaw, I. I.; Wu, A. H.-F.; Lamb, R. N. Influence of Roughness on a Transparent Superhydrophobic Coating. *The Journal of Physical Chemistry C* **2010**, *114* (25), 11228–11233.

(50) Wang, Q.; Sun, G.; Tong, Q.; Yang, W.; Hao, W. Fluorine-Free Superhydrophobic Coatings from Polydimethylsiloxane for Sustainable

Chemical Engineering: Preparation Methods and Applications. *Chemical Engineering Journal* **2021**, *426*, 130829.

(51) Wang, Q.; Sun, G.; Tong, Q.; Yang, W.; Hao, W. Fluorine-Free Superhydrophobic Coatings from Polydimethylsiloxane for Sustainable Chemical Engineering: Preparation Methods and Applications. *Chemical Engineering Journal* **2021**, *426*, 130829.

(52) Zhuang, A.; Liao, R.; Lu, Y.; Dixon, S. C.; Jiamprasertboon, A.; Chen, F.; Sathasivam, S.; Parkin, I. P.; Carmalt, C. J. Transforming a Simple Commercial Glue into Highly Robust Superhydrophobic Surfaces via Aerosol-Assisted Chemical Vapor Deposition. *ACS Appl Mater Interfaces* **2017**, *9* (48), 42327–42335.

(53) Yu, S.; Guo, Z.; Liu, W. Biomimetic Transparent and Superhydrophobic Coatings: From Nature and beyond Nature. *Chemical Communications* **2015**, *51* (10), 1775–1794.

(54) Schardt, L.; Martínez Guajardo, A.; Koc, J.; Clarke, J. L.; Finlay, J. A.; Clare, A. S.; Gardner, H.; Swain, G. W.; Hunsucker, K.; Laschewsky, A. Low Fouling Polysulfobetaines with Variable Hydrophobic Content. *Macromol Rapid Commun* **2022**, *43* (12), 2100589.

(55) Xie, J.; Hu, J.; Lin, X.; Fang, L.; Wu, F.; Liao, X.; Luo, H.; Shi, L. Robust and Anti-Corrosive PDMS/SiO2 Superhydrophobic Coatings Fabricated on Magnesium Alloys with Different-Sized SiO2 Nanoparticles. *Appl Surf Sci* **2018**, *457*, 870–880.

(56) Fürstner, R.; Barthlott, W.; Neinhuis, C.; Walzel, P. Wetting and Self-Cleaning Properties of Artificial Superhydrophobic Surfaces. *Langmuir* **2005**, *21* (3), 956–961.

(57) Geyer, F.; D'Acunzi, M.; Sharifi-Aghili, A.; Saal, A.; Gao, N.; Kaltbeitzel, A.; Sloot, T.-F.; Berger, R.; Butt, H.-J.; Vollmer, D. When and How Self-Cleaning of Superhydrophobic Surfaces Works. *Sci Adv* **2020**, *6* (3), eaaw9727.

(58) Yan, X.; Ji, B.; Feng, L.; Wang, X.; Yang, D.; Rabbi, K. F.; Peng, Q.; Hoque, M. J.; Jin, P.; Bello, E. Particulate–Droplet Coalescence and Self-Transport on Superhydrophobic Surfaces. *ACS Nano* **2022**, *16* (8), 12910–12921.

(59) Milionis, A.; Loth, E.; Bayer, I. S. Recent Advances in the Mechanical Durability of Superhydrophobic Materials. *Adv Colloid Interface Sci* **2016**, *229*, 57–79.

ToC Figure